Article:

Yang, K., Smith, L., Sole, A. et al. (4 more authors) (2019) Supraglacial rivers on the northwest Greenland Ice Sheet, Devon Ice Cap, and Barnes Ice Cap mapped using Sentinel-2 imagery. International Journal of Applied Earth Observation and Geoinformation, 78. pp. 1-13. ISSN 0303-2434

https://doi.org/10.1016/j.jag.2019.01.008

Supraglacial rivers on the northwest Greenland Ice Sheet, Devon Ice Cap, and Barnes Ice Cap mapped using Sentinel-2 imagery

Kang Yang[1,2,3], Laurence C. Smith[4], Andrew Sole[5], Stephen J. Livingstone[5]

Xiao Cheng[2,6], Zhuoqi Chen[2,6], Manchun Li[1,3]

1. School of Geography and Ocean Science, Nanjing University, Nanjing 210023, China
2. Joint Center for Global Change Studies, Beijing 100875, China
3. Jiangsu Provincial Key Laboratory of Geographic Information Science and Technology, Nanjing 210023, China
4. Department of Geography, University of California, Los Angeles, California, USA
5. Department of Geography, The University of Sheffield, Sheffield, S10 2TN, UK
6. State Key Laboratory of Remote Sensing Science, College of Global Change and Earth System Science, Beijing Normal University, Beijing 100875, China

Corresponding author: Kang Yang, Tel: +86-13814179324; Email: yangkangnju@gmail.com

Abstract: Supraglacial rivers set efficacy and time lags by which surface meltwater is routed to the englacial, subglacial, and proglacial portions of ice masses. However, these hydrologic features remain poorly studied mainly because they are too narrow (typically <30 m) to be reliably delineated in conventional moderate-resolution satellite images (e.g., 30 m Landsat-8 imagery). This study demonstrates the utility of 10 m Sentinel-2 Multi-Spectral Instrument images to map supraglacial rivers on the northwest Greenland Ice Sheet, Devon Ice Cap, and Barnes Ice Cap, covering a total area of ~ 10,000 km^2. Sentinel-2 and Landsat-8 both capture overall supraglacial drainage patterns, but Sentinel-2 images are superior to Landsat-8 images for delineating narrow and continuous supraglacial rivers. Sentinel-2 mapping across the three study areas reveals a variety of supraglacial drainage patterns. In northwest Greenland near Inglefield Land, subparallel supraglacial rivers up to 55 km long drain meltwater directly off the ice sheet onto the proglacial zone. On the Devon and the Barnes ice caps, shorter supraglacial rivers (up to 15 – 30 km long) are commonly interrupted by moulins, which drain internally drained catchments on the ice surface to subglacial systems. We conclude that Sentinel-2 offers strong potential for investigating supraglacial meltwater drainage patterns and improving our understanding of the hydrological conditions of ice masses globally.

Key terms: river remote sensing, supraglacial river, surface hydrology, Sentinel-2, Landsat-8, Greenland Ice Sheet

1. Introduction

Supraglacial river networks are one of the least studied hydrologic systems on Earth. Extensive, complex supraglacial river networks have been observed in the ablation zone of the southwest Greenland Ice Sheet (GrIS) (Thomsen et al., 1989; McGrath et al., 2011; Yang and Smith, 2013; Lampkin and VanderBerg, 2014; Poinar et al., 2015; Smith et al., 2015; Yang and Smith, 2016a; Koziol et al., 2017; Smith et al., 2017), the Antarctic Ice Sheet (Bell et al., 2017; Kingslake et al., 2017), some large ice caps/fields (e.g., Devon Ice Cap (Dowdeswell et al., 2004; Boon et al., 2010), and Juneau Ice Field (Marston, 1983; Karlstrom et al., 2014)) as well as smaller stream systems on many mountain glaciers (Stenborg, 1968; Hambrey, 1977; Knighton, 1985; Brykała, 1998; Rippin et al., 2015; Decaux et al., 2018). These surface drainage features impact the efficacy and speed of meltwater routing to the englacial, subglacial, and proglacial portions of glaciers and ice sheets (Stenborg, 1968; Marston, 1983; Smith et al., 2017; Decaux et al., 2018) and thus coupling processes of surface melt with subglacial hydrology and ice flow (Zwally et al., 2002; Bartholomew et al., 2011; Andrews et al., 2014; Poinar et al., 2015; Smith et al., 2015; Wyatt and Sharp, 2015; Karlstrom and Yang, 2016; Yang and Smith, 2016a; Smith et al., 2017). Where meltwater accumulates on ice shelves, hydrofracture of surface crevasses can trigger their rapid collapse, causing debuttressing and acceleration of upstream glaciers (Scambos et al., 2000; Scambos et al., 2003). Active drainage of supraglacial rivers across ice shelves may conversely export stored meltwater and thus prevent disintegration (Bell et al., 2017).

Mapping supraglacial rivers is a crucial task for understanding their hydrological and glaciological roles (Chu, 2014). However, their reliable delineation from remotely sensed imagery is complicated by narrow channel widths relative to typical image resolutions, variable contrast between supraglacial meltwater and the surrounding snow/firn/ice, and complex surface drainage patterns (McGrath et al., 2011; Yang and Smith, 2013; Smith et al., 2017; Yang et al., 2017). Landsat-7/8 images (spatial resolution 15-30 m) have been used to map trunk main-stems of large supraglacial rivers on the Greenland and Antarctic ice sheets (Lampkin and VanderBerg, 2014; Poinar et al., 2015; de Fleurian et al., 2016; Yang and Smith, 2016a; Bell et al., 2017; Kingslake et al., 2017). However, numerous supraglacial rivers are just ~10 m wide (Yang et al., 2016) rendering the spatial resolution of Landsat-7/8 images inadequate for reliable small river delineation. As a result, supraglacial drainage patterns of most ice masses still remain unmapped (Chu, 2014). Very high resolution (VHR) satellite or unmanned aerial vehicle (UAV) images are able to delineate extensive small supraglacial streams (Smith et al., 2017; Yang et al., 2018) but small streams are commonly ignored in most supraglacial hydrologic studies (Lampkin and VanderBerg, 2014; Poinar et al., 2015; Yang and Smith, 2016a; Kingslake et al., 2017). Furthermore, the VHR images are not freely available and are spatially and temporally sparse (McGrath et al., 2011; Yang and Smith, 2013; Rippin et al., 2015; Smith et al., 2017).

The launch of the Sentinel-2 satellites (spatial resolution 10 m) in 2015 and 2017 for the first time raises prospects for studying the overall drainage pattern of supraglacial river networks and derivation of detailed metrics on their distribution, form, and morphology at an appropriate spatial and temporal scale, allowing mapping across large areas with a nominal return frequency of 5-10 days.

This study uses 10 m Sentinel-2 satellite imagery to delineate and map supraglacial river networks on three poorly-studied ice surfaces, the northwest GrIS near Inglefield Land, the Devon Ice Cap, and the Barnes Ice Cap (Figure 1). The potential of 10 m Sentinel-2 images to map surface water masks (Du et al., 2016), and glacier extent and ice flow (Kääb et al., 2016; Paul et al., 2016) have been analyzed, but to our knowledge, this is the first attempt to use Sentinel-2 images to map supraglacial rivers. Therefore, the study's main objectives are to: (1) assess the capability of 10 m Sentinel-2 images to map supraglacial rivers; (2) compare delineations of supraglacial rivers mapped from Sentinel-2 images with those mapped from contemporaneous Landsat-8 images; and (3) characterize the supraglacial river networks on the ice surface of three poorly-studied ice masses.

2. Data

Sentinel-2 is a European Satellite Agency wide-swath, high-resolution, multi-spectral imaging satellite mission (Kääb et al., 2016). This mission consists of two satellites (2A launched on 23 June 2015, and 2B launched on 7 March 2017) flying in the same orbit but phased at 180°, each carrying a single sensor payload named Multi-Spectral Instrument (MSI). MSI includes 13 spectral bands in visible and near-infrared (VNIR) and shortwave Infrared (SWIR). The spatial resolution of these bands varies from 10 m to 60 m. The 10 m bands include blue (band 2, 490 nm), green (band 3, 560 nm), red (band 4, 665 nm), and NIR (band 8, 842 nm), affording mapping of relatively narrow supraglacial rivers. The Level-1C Sentinel-2 product was obtained from the USGS EarthExplorer (http://earthexplorer.usgs.gov/). This product shows the top-of-atmosphere reflectance in cartographic geometry and is divided into 100 km^2 tiles. Several concurrent Landsat-8 OLI images (30 m multi-spectral and 15 m panchromatic images) were also obtained from the USGS EarthExplorer and were used for comparison. Late July or early August images were selected because supraglacial river networks are best-developed on the surface of Arctic ice masses during this period (Table 1).

3. Study area

3.1 Northwest GrIS near Inglefield Land

The southwest GrIS has received the most attention from ice sheet supraglacial hydrologic studies in recent years (McGrath et al., 2011; Lampkin and VanderBerg, 2014; Poinar et al., 2015; Smith et al., 2015; Gleason et al., 2016; Yang and Smith, 2016a; Yang et al., 2016; Smith et al., 2017; Yang et al., 2017). Extensive, complex supraglacial river networks have been observed and mapped from 0.5-2.0 m WorldView (McGrath et al., 2011; Yang and Smith, 2013; Smith et al., 2015; Yang et al., 2016; Koziol et al., 2017; Smith et al., 2017; Yang et al., 2017) and 15-30 m Landsat-7/8 images (Lampkin and VanderBerg, 2014; Poinar et al., 2015; de Fleurian et al., 2016; Yang and Smith, 2016a). These supraglacial river networks drain large volumes of meltwater into the ice sheet (Smith et al., 2015) with important implications for ice dynamics (Zwally et al., 2002; Bartholomew et al., 2011; Andrews et al., 2014; Wright et al., 2016).

Outside of southwest Greenland, the surface hydrology of other areas of the GrIS has received scant attention, resulting in a correspondingly poor understanding of the spatial distribution of hydrologic elements and couplings between surface melt and ice flow (Banwell et al., 2016; Yang and Smith, 2016a).

The northwest GrIS is comprised of predominantly cold-bedded (MacGregor et al., 2016) and slower moving ice (Joughin et al., 2010). Previous studies have revealed wide distributions of supraglacial lakes (mapped from low-resolution MODIS images) (Selmes et al., 2011), indicating that a supraglacial hydrologic system does develop in this area thus contributing to surface mass loss. However, a preliminary investigation of the supraglacial drainage pattern has yet to be conducted.

To address this knowledge gap, we selected a study area on a lobe of slow-moving (~ 0 – 30 m/year) (Joughin et al., 2017) grounded ice from 78.1º to 79.0º N, 64.1º to 69.0º W near Inglefield Land in northwestern Greenland, covering approximately 5,239 km^2 in area including the entire ablation zone and parts of the accumulation zone (equilibrium line altitude is ~1100 m in this area (Box et al., 2004)) (Figure 1 and 2). Ice surface elevation in this study area ranges from 200 to 1500 m a.s.l., sloping gently (~0.015 m/m) to the ice edge. A Global 30 Arc-Second Elevation (GTOPO30) digital elevation model (obtained from the USGS EarthExplorer) was used to create elevation contours.

3.2 Devon Ice Cap

The Devon Ice Cap (DIC) is a polythermal Arctic ice cap and one of the largest ice masses in the Canadian Arctic. It is located between 74.5º to 75.8º N, 80.0º to 86.0º W and covers an area of ~14,400 km^2 (Boon et al., 2010) (Figure 1). The DIC has a dome-like shape with ice divides radiating from its summit (elevation ~1921 m) (Dowdeswell et al., 2004). We selected two study sites from the southern and western sections of the DIC (Figure 3) that are representative of the broader ice cap flow and hydrology (Dowdeswell et al., 2004; Boon et al., 2010; Wyatt and Sharp, 2015). The southern site (Figure 3c) has an area of 621 km^2 with elevations ranging from 800 to 1300 m. The western site (Figure 3b) has an area of 200 km^2 and ranges in elevation from 500 to 1400 m. The southern site is drained by several large outlet glaciers and is characterized by relatively fast ice flow velocities (~ 10 – 60 m/year). Closely-spaced supraglacial river networks have been observed in this area (Dowdeswell et al., 2004) and were previously mapped for one outlet glacier using Landsat-7 ETM+ imagery (Wyatt and Sharp, 2015). The western study site is flatter than the southern site and flows more slowly (~5 m/year). It has received less attention compared to its fast-flowing southern counterpart (Dowdeswell et al., 2004).

3.3 Barnes Ice Cap

The Barnes Ice Cap (BIC) is a remnant of the Laurentide Ice Sheet (Gilbert et al., 2016) located in central Baffin Island, Canada. It covers an area of ~5700 km^2 from approximately 69.5º to 70.5º N, 71.8º to 74.8º W (Figure 1). The BIC is very sensitive to Arctic climate change and is predicted to disappear in the next 300 years (Gilbert et al., 2017). Like the DIC, the BIC also has a dome-like shape but its ice divide mainly runs northwest – southeast (Figure 4). Research on the BIC has focused mainly on its accelerated melting and thinning in response to climate warming and internal dynamics (Dupont et al., 2012; Gilbert et al., 2016; Gilbert et al., 2017). BIC hydrology, in contrast, has received scant attention and to our knowledge, no study of BIC supraglacial streams and rivers has been conducted to date.

4. Methods

Effective delineation of supraglacial rivers from remotely sensed images requires linear feature enhancement. For this we employed the method of Yang et al. (2017), which characterizes rivers according to their Gaussian-like brightness cross sections and longitudinal continuity. First, the normalized difference water index (NDWI) was applied to enhance the spectral contrast between meltwater and background snow/ice (Yang and Smith, 2013). Second, a band-pass Discrete Fourier Transform (DFT) was used to further remove the low-frequency image background and high-frequency image noise (Yang et al., 2017). A band-pass filter ramped between 1/200 m^{-1} and 1/40 m^{-1} was found to effectively remove image background and high-frequency image noise, while retaining supraglacial rivers as the dominant features on the ice sheet surface (Karlstrom and Yang, 2016). Third, a Gabor filter was used to enhance supraglacial river cross sections (Yang et al., 2015a). The Gabor filter is a sinusoidally-modulated Gaussian function with optimal localization for matching river cross sections that effectively enhances supraglacial river features relative to the surrounding snow/firn/ice surface background.

Even after Gabor filtering, supraglacial rivers often appear intermittent owing to significant visible/near-infrared brightness variations along river courses and snow bridges (snow-filled channels, with a supraglacial stream or river actively flowing beneath). To address this problem, a flexible path opening operator (Heijmans et al., 2005) was used to lengthen the river channel continuity and to suppress noise. Rivers were consistently discerned from the image background after these steps. Finally, a global threshold was automatically determined based on the image histogram and applied to create binary river masks (Yang et al., 2015a). These supraglacial river detection codes are freely available by contacting the lead author.

Moulins were manually identified as the abrupt termination of a large river main-stem (Smith et al., 2015; Wyatt and Sharp, 2015; Yang and Smith, 2016a). To be conservative, only moulins close to crevasses or drained channels and that clearly terminate river networks were identified. River widths vary longitudinally so it is common for some river segments to still be too narrow in 10 m Sentinel-2 images, inducing false river terminations. Therefore, if a supraglacial river ends but then reappears a short distance downstream with similar width, the upstream river termination is not identified as a moulin. This step also mitigates for presence of snow bridges, which can conceal supraglacial rivers for tens to hundreds of meters.

5. Results

5.1 Comparison of Sentinel-2 and Landsat-8 mapped supraglacial rivers

Supraglacial river networks are better delineated in 10 m Sentinel-2 images than the 30 m multispectral or 15 m panchromatic Landsat-8 data (Figure 5) and can be efficiently detected using Gabor filtering and path opening (Figure 6). Supraglacial river networks were mapped for the northwest GrIS, the DIC, and the BIC using near-time Sentinel-2 and Landsat-8 images captured during 2016 summer (Figure 7 – 9, Table 2). The total area mapped is ~10,000 km^2, with well-developed supraglacial river networks found on all three ice masses. Both Sentinel-2 and Landsat-8 images captured the overall drainage pattern of supraglacial river networks on the ice surface of the three study areas (Figure 7 – 9), supporting the conclusions that moderate-resolution satellite images hold value for studying ice surface drainage patterns (Lampkin and VanderBerg, 2014; Poinar et al., 2015; Yang and Smith, 2016a; Bell et al., 2017; Kingslake et al., 2017). However, the spatial resolution of the Sentinel-2 images is three times higher than that of the Landsat-8 images and thus supraglacial drainage patterns are much better resolved in the Sentinel-derived map products (see close-up images, Figures 7 – 9). Sentinel-mapped supraglacial river networks are also more continuous, which is crucial for investigating surface meltwater routing (King et al., 2016; Yang and Smith, 2016a; Smith et al., 2017; Decaux et al., 2018; Yang et al., 2018). On all three ice masses, supraglacial rivers generally flow from high-elevation slushy zones to low-elevation bare ice ablation zones. In the slushy zones, supraglacial rivers are not clearly channelized, yet the Sentinel-2 images were nevertheless able to discern the short, often braided river networks in three areas whereas these features were difficult to identify in Landsat-8 (see Figure 7).

Drainage density (D_d) was calculated to characterize the overall abundance of supraglacial rivers across the three study sites (Table 2). The derived values of D_d are highly sensor-specific, with Sentinel-derived D_d (2.5 – 5.6 km^{-1}) approximately two times higher than Landsat-derived values (1.3 – 2.7 km^{-1}). The highest D_d (5.6 km^{-1}) was obtained on the northwest GrIS during late July 2016, indicating a well-developed supraglacial drainage system despite having the highest latitude of the three areas (Figure 7). The western and southern areas of the DIC yielded D_d values of 5.1 km^{-1} and 3.3 km^{-1} respectively, indicating denser surface drainage in the west (Figure 8), consistent with previous studies (Dowdeswell et al., 2004; Boon et al., 2010). The BIC exhibited the lowest D_d (2.5 km^{-1}), mainly due to a large river-free area near the ice margin (Figure 9), but also because the Sentinel-2 images used to map the BIC were acquired in mid-August, when surface melt declines and actively flowing supraglacial river networks generally shrink (Yang and Smith, 2016a; Yang et al., 2018).

5.2 Supraglacial river networks on the northwest Greenland Ice Sheet

Supraglacial river networks on the northwestern GrIS near Inglefield Land drain meltwater directly off the ice surface into proglacial streams and rivers (Figure 7). These mapped supraglacial rivers are subparallel (spacing ~200 m) and reach a maximum length of ~65 km, longer than the longest main-stem (~55 km) previously mapped on the southwest GrIS (Poinar et al., 2015). This subparallel drainage pattern is also very different from the generally dendritic and/or structurally controlled patterns observed in southwest Greenland (Smith et al., 2015; Karlstrom and Yang, 2016; Yang and Smith, 2016a; Yang et al., 2016) and flow continuously straight off the ice sheet surface from the interior (elevation ~1500 m) to its edge (elevation ~200 m) (Figure 7). These features originate in slush fields at high elevations (~1500 m) where they are not well channelized, becoming well channelized at lower elevations on bare ice. Importantly, none of the Inglefield Land supraglacial rivers are interrupted by moulins or crevasses making this area distinctly different from southwest Greenland, where virtually all supraglacial rivers terminate in moulins before reaching the ice edge (Smith et al., 2015; Yang and Smith, 2016a).

Although the supraglacial drainage patterns of the two study sites are both continuous (Figure 7b and 7c), notable differences can be observed. At site b, supraglacial rivers are subparallel, straight and densely distributed, and supraglacial lakes are absent (Figure 7b). At site c, supraglacial rivers flow into and out of supraglacial lakes (termed as “pathway” lakes in southwest GrIS studies (Tedesco et al., 2013; Yang et al., 2015b)) forming “lake chains” and a more sinuous supraglacial river network (Figure 7c), whereas supraglacial lakes are absent at site b. This difference is induced by broad-scale ice surface topography; elevation contours at site b are subparallel, while the contours at site c are more irregular, particularly near supraglacial lakes.

5.3 Supraglacial river networks on the Devon Ice Cap

The supraglacial river drainage pattern on the southern section of the DIC is strongly controlled by moulins and crevasses. At this site, most supraglacial rivers drain southwards along an outlet glacier, reaching a maximum length of ~15 km. At higher elevations (~1300-1400 m a.s.l.) most of the mapped river channels are very narrow (one pixel wide), braided, and slushy, similar to their high elevation (>1500 m) counterparts on the southwest GrIS (Yang and Smith, 2016a). The drainage density is high where meltwater channelizes but there are also large interfluves with no channels. Supraglacial rivers in this area, particularly the main tributaries, are very sinuous and often turn at right angles (Figure 8). Consistent with previous findings (Dowdeswell et al., 2004), crevasses are identified in this area, which abruptly terminate supraglacial rivers to form moulins (Figure 8).

All of the supraglacial river networks mapped in the southern section of the DIC are captured by moulins, similar to the southwest GrIS (Smith et al., 2015). For example, 16 moulins (density 0.08 moulin/km^2, calculated as moulin count / study site area) in the lower-middle part of the study site correspond to a ~3 km long west-east orientated linear crevasse. Another isolated moulin was found nearby draining a very large supraglacial river network (see the right yellow box in Figure 8). These widely distributed moulins drain large volumes of meltwater into the ice cap and likely play a significant role in coupling surface melt with the subglacial hydrological system and ice flow (Zwally et al., 2002; Banwell et al., 2013; Andrews et al., 2014; Clason et al., 2015; Wyatt and Sharp, 2015) of the DIC. The resultant moulin density (0.08 moulin/km^2) is similar to the density reported for low-elevation (<1400 m) southwestern GrIS (>0.06 moulin/km^2) (Yang and Smith, 2016a), indicating that moulins on the southern section of the DIC are as abundant as their southwest GrIS counterparts in general.

Supraglacial river networks are well developed on the western section of the DIC, with most rivers flowing continuously toward the ice margin (Figure 8). At high elevations, we mapped numerous supraglacial rivers yielding correspondingly high drainage densities (D_d = 5.1 km^{-1}). These supraglacial rivers are straighter than their counterparts in the southern section of the DIC. At lower elevations (<900 m), supraglacial rivers become sinuous and are captured by ~10 main-stems, forming a limited number of large supraglacial river networks (Figure 8). A large, previously unreported low albedo zone is found in this low-elevation area (Figure 3 and 8). A previous field study during 1998 also observed well-developed supraglacial rivers with long main-stems in this area and thereby assumed surface-to-bed meltwater connections were limited (Lamoureux et al., 2002; Boon et al., 2010). However, we mapped a total of 16 moulins (density 0.03 moulin/km^2) and most moulins are located close to the ice margin (<3 km), thus terminating relatively large river networks (10–20 km long main-stems). This new finding indicates a considerable volume of meltwater can be drained into the lower ice margin of the western section of the

DIC, which is contrary to previous assumptions and implies either recent moulin formation or spatial limitations of the field observations.

5.4 Supraglacial river networks on the Barnes Ice Cap

Supraglacial river networks were mapped across the entire BIC using both Sentinel-2 and Landsat-8 (Figure 9). Supraglacial rivers drain ~30 km towards the southwestern and ~22 km towards the northeastern portions of the ice cap, flowing away from the 128 km long northwest-southeast trending ice divide. The longest supraglacial river on the western side is ~35 km, and the longest on the eastern side is ~25 km, both governed by the distances from the ice margins to the ice divide (Figure 9).

There are noticeable differences between the drainage patterns on either side of the BIC ice divide. On the eastern side, supraglacial rivers are relatively straight and subparallel, similar to the northwestern GrIS (Figure 7) and the western section of the DIC (Figure 8). On the western side, they are more dendritic (similar to the southern section of the DIC, Figure 8). On both sides numerous supraglacial rivers drain directly into proglacial lakes and rivers. However, some also terminate abruptly in moulins (Figure 9), indicating that some meltwater does reach the BIC bed. A total of 66 moulins (density 0.01 moulin/km^2, calculated as moulin count / BIC area) were identified from the Sentinel-2 images, of which 27 (density 0.01 moulin/km^2, calculated as moulin count / the western BIC area) were detected west of the divide and 39 (density 0.02 moulin/km^2, calculated as moulin count / the eastern BIC area) east of the divide. Most moulins are located close to the BIC ice margin (5–7 km) and thus terminate relatively large supraglacial river networks (15–25 km long main-stems) relatively close to the proglacial zone.

6. Discussion

6.1 Scientific implications of observed supraglacial drainage patterns

This study maps supraglacial river networks on three poorly-studied ice masses, the northwestern GrIS near Inglefield Land, the Devon Ice Cap, and the Barnes Ice Cap using 10 m Sentinel-2 and Landsat-8 satellite imagery. A variety of supraglacial drainage patterns is revealed. On the northwestern

GrIS, on high-elevation areas of the western sections of the DIC and the BIC, and on the eastern section of the BIC, supraglacial rivers are straight, subparallel, and densely distributed (Figure 7-9) indicating limited variations in surface relief (Karlstrom and Yang, 2016; Crozier et al., 2018; Ignéczi et al., 2018). In contrast, the southern section of the DIC and the low-elevation areas of the western sections of the DIC and the BIC have supraglacial river drainage patterns that are more dendritic, (Figure 8 and 9), similar to the southwest GrIS (Smith et al., 2015; King et al., 2016; Yang et al., 2016; Smith et al., 2017) and many terrestrial river systems (Dingman, 2015), indicating relatively large variations in surface relief and greater transfer of basal roughness and slipperiness (Crozier et al., 2018; Ignéczi et al., 2018). There is also considerable variation within some of the study sites. For example, on the western sections of the DIC and the BIC, subparallel supraglacial rivers developed at high elevations become more sinuous and dendritic downstream and are eventually captured by highly sinuous main-stems (Figure 8).

Supraglacial drainage patterns are primarily determined by ice surface topography, which is influenced by variations in bed roughness and slipperiness and the differing transmission of that variability to the ice surface (Crozier et al., 2018; Ignéczi et al., 2018). Therefore, inversely, satellite-mapped supraglacial river networks hold useful information for inferring subsurface topography and basal transfer characteristics. Regional and local variations in supraglacial river pattern are consistent with theory and observations that the transfer of basal variability is enhanced by thinner ice, steeper ice surface slopes and higher slip ratios prevalent in ice-marginal and fast-flowing regions (Gudmundsson, 2003; Crozier et al., 2018; Ignéczi et al., 2018). More generally, there is a propensity of all natural rivers to adjust their own slope (i.e. to decrease it, in this case) through increasing their sinuosity (Charlton, 2007). Finally, crevasses, which tend to be associated with faster flowing and thinner ice (Colgan et al., 2011), fragment supraglacial rivers networks and generate moulins (Yang and Smith, 2016a). As a result, low-elevation supraglacial rivers near the ice edge are not well channelized for the DIC and the BIC, yielding short river segments and moulins (Figure 8 and 9). In contrast, on cold bedded northwestern GrIS with slow ice flow (Joughin et al., 2010), crevasses are rare and therefore long supraglacial rivers flow continuously straight off the ice sheet surface (Figure 7).

6.2 Implications for surface meltwater routing

The supraglacial drainage patterns mapped in this study have important implications for surface meltwater routing. Supraglacial river networks and their corresponding ice surface catchments determine the timing and magnitude of peak supraglacial river discharge and corresponding inputs to englacial and subglacial drainage systems through moulins (Smith et al., 2017; Decaux et al., 2018; Yang et al., 2018). Various factors control how a supraglacial river's hydrograph responds to ice surface melt, including catchment shape, contributing area, drainage density, ice surface properties (snow/firn/weathering crust/ice), surface melt rate, and surface topographic gradient (Arnold et al., 1998; Leeson et al., 2012; Banwell et al., 2013; Clason et al., 2015; Smith et al., 2017; Yang et al., 2018). Integration of regional climatic models (RCMs), satellite observations, high-quality DEMs and fieldwork are required to conduct a comprehensive investigation of catchment hydrological responses (Smith et al., 2015; Yang and Smith, 2016a; Smith et al., 2017), which is outside the scope of this study. However, of these controlling factors, catchment area and shape are the most straightforward to acquire and most stable over time (Yang and Smith, 2016a; Smith et al., 2017). Therefore, a basic understanding of catchment hydrological responses to catchment shape can be obtained from remotely sensed mapped supraglacial river networks, if other controlling factors are assumed to be constant. We acknowledge that this may oversimplify reality but argue it provides a preliminary understanding of catchment hydrological response to meltwater generation on ice surfaces.

On the northwestern GrIS and eastern section of the BIC, the straight and subparallel supraglacial river networks yield unusually long and narrow catchments (Yang and Smith, 2016a). As a result, it takes longer on average for meltwater to travel to the catchment outlet and the supraglacial catchment output runoff hydrograph will be more subdued with a longer rising limb (Karamouz et al., 2013). Because these supraglacial rivers flow directly onto the proglacial zone (Figure 2 and 7) discharge into terrestrial streams and rivers directly reflects the timing and intensity of ice surface runoff influenced by catchment routing, with no modulation by en- and/or subglacial processes. In contrast, the dendritic supraglacial river networks on the southern section of the DIC, similar to their counterparts on the southwest GrIS (Yang and Smith, 2016a), have more compact (more circular rather than long and narrow) catchment shapes and the resultant runoff hydrograph will be more flashy with a greater peak and shorter rising limb (Smith et al., 2017). On the western sections of the DIC and the BIC, where subparallel and dendritic drainage patterns both exist, the runoff hydrographs are expected to be complex composites of the aforementioned subdued and flashy hydrographs (Karamouz et al., 2013).

Drainage density (D_d) of supraglacial rivers also controls the hydrological responses of supraglacial catchments but D_d varies significantly over a melt season (Yang et al., 2017). For a given catchment, high drainage density will lead to flashy drainage since open-channels route surface meltwater much more efficiently (10^{-1} m/s) than hillslope overland/subsurface flow (10^{-3}-10^{-4} m/s) (Yang et al., 2018). However, 10 m Sentinel-2 mapped drainage density cannot detect small supraglacial streams and thus likely underestimates the extent of high drainage density, hydraulically efficient catchment. Moreover, it is inappropriate to directly compare D_d derived for different ice masses during different time periods. Further study is needed to determine the usefulness of Sentinel-2 mapping of drainage density and surface meltwater routing studies more generally.

6.3 Implications for coupling with subglacial systems

Remotely sensed supraglacial drainage patterns provide improved understanding of the coupling between supraglacial hydrology and subglacial systems. The long, subparallel supraglacial rivers of the northwest GrIS are very different from those in the southwest, which are characterized by numerous segmented river networks terminating at moulins (Poinar et al., 2015; Smith et al., 2015; King et al., 2016; Yang and Smith, 2016a; Yang et al., 2016; Ignéczi et al., 2018). We suggest relatively cold, thick, and broadly impermeable ice, slow flow, and low strain rates (Rignot and Kanagaratnam, 2006; Joughin et al., 2016) all contribute to the absence of moulins and crevasses in northwest Greenland. As a result, the coupling between surface hydrology and ice flow is likely weak, with ice motion in this region dominated by internal deformation (Boon et al., 2010), similar to findings reported for the Antarctic Ice Sheet (Bell et al., 2017; Kingslake et al., 2017).

Considerable numbers of moulins are found on the western sections of the DIC and the BIC, places where moulins have previously been considered rare and the coupling between surface hydrology and ice flow remains unstudied (Dowdeswell et al., 2004; Boon et al., 2010; Gilbert et al., 2016). This new finding indicates that non-trivial volumes of meltwater drain into the two ice caps each summer. Wyatt and Sharp (2015) mapped moulins for an outlet glacier (<600 m) in the south sector of the DIC and found that ice velocity variability is greater near moulins. Through our expanded mapping, we find that moulins are widely distributed in the high-elevation (>800 m) interior of the southern section of the DIC. This is similar to southwestern GrIS, where moulins are widely distributed inland (e.g., >100 km to the ice margin) (Yang and Smith, 2016a) and drain short supraglacial rivers near the ice margin (~4 km long main-stems) (Poinar et al., 2015). In contrast, most moulins identified for the western sections of the DIC and the BIC are located close to the ice margin (~5 km) and drain long supraglacial river networks (10-25 km long main-stems), indicating substantial ability to drain meltwater into the ice cap but limited overall coupling with ice dynamics given the relatively small area of the bed that is hydraulically connected to the ice surface. This unique coupling may lead to a strong response of marginal ice flow to surface meltwater inputs but the effect of supraglacial meltwater on inland ice flow may be weak.

6.4 Limitations and future potential of Sentinel-2 for supraglacial river mapping

Although higher-resolution satellite (e.g., WorldView-1/2) (McGrath et al., 2011; Joughin et al., 2013; Yang and Smith, 2013; Smith et al., 2015; Smith et al., 2017; Yang et al., 2017) and UAV images (Rippin et al., 2015; Smith et al., 2017) can detect very small supraglacial streams, Sentinel-2 images provide a promising spatial scale to map larger supraglacial river networks over large areas (Figure 7-9). This is crucial for accurately delineating internally drained catchments (IDCs) (Yang and Smith, 2016a; Smith et al., 2017), which directly control the timing and magnitude of surface meltwater inputs into ice masses (Banwell et al., 2013; Clason et al., 2015; Smith et al., 2015; Smith et al., 2017) and cannot be readily determined from DEMs (Yang and Smith, 2016b). Furthermore, as reported in Yang and Smith (2016a), supraglacial rivers as narrow as ~3 m are sometimes distinguishable in 15 m Landsat-8 images if the surrounding ice surface is bright and clean, creating strong contrast with dark supraglacial rivers. Under such conditions, Sentinel-2 images may therefore detect even narrower, higher-order supraglacial streams (Yang et al., 2016), thus characterizing ice surface drainage patterns more comprehensively.

The distribution of dark dust (low albedo) zones influences the quality of Sentinel-2 supraglacial river maps. These zones are typically found <10 km from the western ice margin of the DIC and pose a challenge for distinguishing supraglacial rivers against the surrounding dark background (Figure 3b). Supraglacial rivers are not well channelized in this area and thus cannot be enhanced by the river detection algorithm presented here. For this reason, low-elevation (<900 m) supraglacial rivers are not well detected and drainage density at low elevations appears to decrease dramatically after flowing into the dark dust zone (Figure 10), which is likely erroneous. We therefore suggest caution when mapping supraglacial rivers or drainage densities using moderate-resolution Sentinel-2 imagery in areas of dark ice.

Integrating remotely sensed river mapping with DEM data will further improve our understanding of supraglacial drainage patterns. Moderate-resolution (30 m) DEMs have been integrated with remotely sensed mapping to study the fluvial-morphometry of supraglacial meltwater channels in southwestern Greenland (Yang et al., 2015b; Yang et al., 2016). The availability of high spatial resolution (~2-5 m) DEMs (e.g., ArcticDEM (Noh and Howat, 2015, 2017)) raises prospects for studying surface meltwater channel morphometry in unprecedented detail. In Yang et al. (2018), a 3 m resolution DEM was utilized to simulate seasonal evolution of supraglacial river networks with a series of cumulative contributing area thresholds. By integrating ArcticDEM-simulated continuous drainage networks with image-mapped supraglacial river networks it becomes possible to create a single river product containing numerous hydraulically useful channel characteristics (e.g., length, width, slope, sinuosity, and stream order). A preliminary example is shown in Figure 11. ArcticDEM-simulated drainage networks are more continuous than Sentinel-2 supraglacial river networks but the method struggles to reproduce river distribution (overestimating high-elevation rivers, underestimating low-elevation rivers, and failing to identify moulins).

7. Conclusions

As satellite sensor spatial and temporal resolutions continue to improve, supraglacial streams and rivers are increasingly discernible on various different snow, firn and ice surfaces. The twin Sentinel-2 satellites (2A and 2B) began accumulating global coverage in 2017 with a short revisit time (~5 days) and 10 m spatial resolution. This paper has provided a first synoptic mapping of supraglacial river drainage networks on the northwest Greenland Ice Sheet near Inglefield Land, the Devon Ice Cap, and the Barnes Ice Cap using these data. Based on this demonstration, we conclude that the growing Sentinel-2 archive will enable mapping of supraglacial river drainage networks, their termination points, and seasonal and inter-annual evolution for ice masses globally. Remotely sensed drainage networks will advance understanding of meltwater source areas and routing pathways on large ice masses, while their termination locations will help to identify areas of hydrological coupling between ice surfaces and subglacial systems.

Acknowledgements

Kang Yang acknowledges support from the National Natural Science Foundation of China (41871327), the National Key R&D Program (2018YFC1406101), and the Fundamental Research Funds for the Central Universities. Laurence C. Smith acknowledges the support of the NASA Cryosphere Program managed by Dr. Thomas Wagner. Stephen Livingstone and Andrew Sole acknowledge the support of a White Rose University Consortium Collaboration Fund grant.

References

Andrews, L.C., Catania, G.A., Hoffman, M.J., Gulley, J.D., Luthi, M.P., Ryser, C., Hawley, R.L., Neumann, T.A., 2014. Direct observations of evolving subglacial drainage beneath the Greenland Ice Sheet. Nature 514, 80-83.

Arnold, N.S., Richards, K., Willis, I., Sharp, M., 1998. Initial results from a distributed, physically based model of glacier hydrology. Hydrol. Process. 12, 191-219.

Banwell, A.F., Hewitt, I., Willis, I., Arnold, N., 2016. Moulin density controls drainage development beneath the Greenland ice sheet. J. Geophys. Res. Earth Surf. 121, 2248-2269.

Banwell, A.F., Willis, I.C., Arnold, N.S., 2013. Modeling subglacial water routing at Paakitsoq, W Greenland. J. Geophys. Res. Earth Surf. 118, 1282-1295.

Bartholomew, I., Nienow, P., Sole, A., Mair, D., Cowton, T., Palmer, S., Wadham, J., 2011. Supraglacial forcing of subglacial drainage in the ablation zone of the Greenland ice sheet. Geophys. Res. Lett. 38.

Bell, R.E., Chu, W., Kingslake, J., Das, I., Tedesco, M., Tinto, K.J., Zappa, C.J., Frezzotti, M., Boghosian, A., Lee, W.S., 2017. Antarctic ice shelf potentially stabilized by export of meltwater in surface river. Nature 544, 344-348.

Boon, S., Burgess, D.O., Koerner, R.M., Sharp, M.J., 2010. Forty-seven Years of Research on the Devon Island Ice Cap, Arctic Canada. Arctic 63, 13-29.

Box, J.E., Bromwich, D.H., Bai, L.S., 2004. Greenland ice sheet surface mass balance 1991–2000: Application of Polar MM5 mesoscale model and in situ data. J. Geophys. Res. Atmos. 109.

Brykała, D., 1998. Evolution of supraglacial drainage on Waldemar Glacier (Spitsbergen) in the period 1936–1998, Polish Polar Studies: 25th International Polar Symposium, Inst. Geofiz. PAN, Warsaw.

Charlton, R., 2007. Fundamentals of Fluvial Geomorphology. Routledge.

Chu, V.W., 2014. Greenland ice sheet hydrology: a review. Prog. Phys. Geogr. 38, 19-54.

Clason, C.C., Mair, D.W.F., Nienow, P.W., Bartholomew, I.D., Sole, A., Palmer, S., Schwanghart, W., 2015. Modelling the transfer of supraglacial meltwater to the bed of Leverett Glacier, Southwest Greenland. Cryosph. 9, 123-138.

Colgan, W., Steffen, K., McLamb, W.S., Abdalati, W., Rajaram, H., Motyka, R., Phillips, T., Anderson, R., 2011. An increase in crevasse extent, West Greenland: Hydrologic implications. Geophys. Res. Lett. 38, L18502.

Crozier, J., Karlstrom, L., Yang, K., 2018. Basal control of supraglacial meltwater catchments on the Greenland Ice Sheet. Cryosph. 12, 3383-3407.

de Fleurian, B., Morlighem, M., Seroussi, H., Rignot, E., van den Broeke, M.R., Kuipers Munneke, P., Mouginot, J., Smeets, P.C.J.P., Tedstone, A.J., 2016. A modeling study of the effect of runoff variability on the effective pressure beneath Russell Glacier, West Greenland. J. Geophys. Res. Earth Surf. 121, 1834-1848.

Decaux, L., Grabiec, M., Ignatiuk, D., Jania, J., 2018. Role of discrete recharge from the supraglacial drainage system for modelling of subglacial conduits pattern of Svalbard polythermal glaciers. Cryosph. Discuss.

Dingman, S.L., 2015. Physical hydrology (3rd edition). Waveland press.

Dowdeswell, J.A., Benham, T.J., Gorman, M.R., Burgess, D., Sharp, M.J., 2004. Form and flow of the Devon Island Ice Cap, Canadian Arctic. J. Geophys. Res. Earth Surf. 109.

Du, Y., Zhang, Y., Ling, F., Wang, Q., Li, W., Li, X., 2016. Water Bodies' Mapping from Sentinel-2 Imagery with Modified Normalized Difference Water Index at 10-m Spatial Resolution Produced by Sharpening the SWIR Band. Remote Sens. 8, 354.

Dupont, F., Royer, A., Langlois, A., Gressent, A., Picard, G., Fily, M., Cliche, P., Chum, M., 2012. Monitoring the melt season length of the Barnes Ice Cap over the 1979-2010 period using active and passive microwave remote sensing data. Hydrol. Process. 26, 2643-2652.

Gilbert, A., Flowers, G.E., Miller, G.H., Rabus, B.T., Van Wychen, W., Gardner, A.S., Copland, L., 2016. Sensitivity of Barnes Ice Cap, Baffin Island, Canada, to climate state and internal dynamics. J. Geophys. Res. Earth Surf. 121, 1516-1539.

Gilbert, A., Flowers, G.E., Miller, G.H., Refsnider, K.A., Young, N.E., Radic, V., 2017. The projected demise of Barnes Ice Cap: Evidence of an unusually warm 21st century Arctic. Geophys. Res. Lett. 44, 2810-2816.

Gleason, C.J., Smith, L.C., Chu, V.W., Legleiter, C.J., Pitcher, L.H., Overstreet, B.T., Rennermalm, A.K., Forster, R.R., Yang, K., 2016. Characterizing supraglacial meltwater channel hydraulics on the Greenland Ice Sheet from in situ observations. Earth Surf. Process. Landf.

Gudmundsson, G.H., 2003. Transmission of basal variability to a glacier surface. J. Geophys. Res. Solid Earth 108.

Hambrey, M.J., 1977. Supraglacial drainage and its relationship to structure, with particular reference to Charles Rabots Bre, Okstindan, Norway. Norsk Geografisk Tidsskrift - Norwegian Journal of Geography 31, 69-77.

Heijmans, H., Buckley, M., Talbot, H., 2005. Path openings and closings. J Math Imaging Vis 22, 107-119.

Ignéczi, Á., Sole, A.J., Livingstone, S.J., Ng, F.S., Yang, K., 2018. Greenland Ice Sheet surface topography and drainage structure controlled by the transfer of basal variability. Front. Earth Sci. 6, 101.

Joughin, I., Das, S.B., Flowers, G.E., Behn, M.D., Alley, R.B., King, M.A., Smith, B.E., Bamber, J.L., van den Broeke, M.R., van Angelen, J.H., 2013. Influence of ice-sheet geometry and supraglacial lakes on seasonal ice-flow variability. Cryosph. 7, 1185-1192.

Joughin, I., Smith, B., Howat, I., Scambos, T., 2017. MEaSUREs Greenland Ice Sheet Velocity Map from InSAR Data, Version 2 [2015–2016 subset]. NASA National Snow and Ice Data Center Distributed Active Archive Center

Joughin, I., Smith, B.E., Howat, I.M., Moon, T., Scambos, T.A., 2016. A SAR record of early 21st century change in Greenland. J. Glaciol. 62, 62-71.

Joughin, I., Smith, B.E., Howat, I.M., Scambos, T., Moon, T., 2010. Greenland flow variability from ice-sheet-wide velocity mapping. J. Glaciol. 56, 415-430.

Kääb, A., Winsvold, S., Altena, B., Nuth, C., Nagler, T., Wuite, J., 2016. Glacier Remote Sensing Using Sentinel-2. Part I: Radiometric and Geometric Performance, and Application to Ice Velocity. Remote Sens. 8, 598.

Karamouz, M., Nazif, S., Falahi, M., 2013. Hydrology and hydroclimatology. CRC Press.

Karlstrom, L., Yang, K., 2016. Fluvial supraglacial landscape evolution on the Greenland Ice Sheet. Geophys. Res. Lett. 43, 2683–2692.

Karlstrom, L., Zok, A., Manga, M., 2014. Near-surface permeability in a supraglacial drainage basin on the Llewellyn Glacier, Juneau Icefield, British Columbia. Cryosph. 8, 537-546.

King, L., Hassan, M., Yang, K., Flowers, G., 2016. Flow routing for delineating supraglacial meltwater channel networks. Remote Sens. 8, 988.

Kingslake, J., Ely, J.C., Das, I., Bell, R.E., 2017. Widespread movement of meltwater onto and across Antarctic ice shelves. Nature 544, 349-352.

Knighton, A.D., 1985. Channel form Adjustment in Supraglacial Streams, Austre Okstindbreen, Norway. Arc. Antarct. Res. 17, 451-466.

Koziol, C., Arnold, N., Pope, A., Colgan, W., 2017. Quantifying supraglacial meltwater pathways in the Paakitsoq region, West Greenland. J. Glaciol. 63, 464-476.

Lamoureux, S.F., Gilbert, R., Lewis, T., 2002. Lacustrine Sedimentary Environments in High Arctic Proglacial Bear Lake, Devon Island, Nunavut, Canada. Arct. Antarct. Alp. Res. 34, 130-141.

Lampkin, D.J., VanderBerg, J., 2014. Supraglacial melt channel networks in the Jakobshavn Isbræ region during the 2007 melt season. Hydrol. Process. 28, 6038-6053.

Leeson, A.A., Shepherd, A., Palmer, S., Sundal, A., Fettweis, X., 2012. Simulating the growth of supraglacial lakes at the western margin of the Greenland ice sheet. Cryosph. 6, 1077-1086.

MacGregor, J.A., Colgan, W.T., Fahnestock, M.A., Morlighem, M., Catania, G.A., Paden, J.D., Gogineni, S.P., 2016. Holocene deceleration of the Greenland Ice Sheet. Science 351, 590-593.

Marston, R.A., 1983. Supraglacial stream dynamics on the Juneau icefield. Ann. Assoc. Am. Geogr. 73, 597-608.

McGrath, D., Colgan, W., Steffen, K., Lauffenburger, P., Balog, J., 2011. Assessing the summer water budget of a moulin basin in the Sermeq Avannarleq ablation region, Greenland ice sheet. J. Glaciol. 57, 954-964.

Noh, M.-J., Howat, I.M., 2015. Automated stereo-photogrammetric DEM generation at high latitudes: Surface Extraction with TIN-based Search-space Minimization (SETSM) validation and demonstration over glaciated regions. GIScience & Remote Sensing 52, 198-217.

Noh, M.-J., Howat, I.M., 2017. The Surface Extraction from TIN based Search-space Minimization (SETSM) algorithm. ISPRS J. Photogramm. Remote Sens. 129, 55-76.

Paul, F., Winsvold, S., Kääb, A., Nagler, T., Schwaizer, G., 2016. Glacier Remote Sensing Using Sentinel-2. Part II: Mapping Glacier Extents and Surface Facies, and Comparison to Landsat 8. Remote Sens. 8, 575.

Poinar, K., Joughin, I., Das, S.B., Behn, M.D., Lenaerts, J.T.M., van den Broeke, M.R., 2015. Limits to future expansion of surface-melt-enhanced ice flow into the interior of western Greenland. Geophys. Res. Lett. 42, 1800-1807.

Rignot, E., Kanagaratnam, P., 2006. Changes in the velocity structure of the Greenland ice sheet. Science 311, 986-990.

Rippin, D.M., Pomfret, A., King, N., 2015. High resolution mapping of supra-glacial drainage pathways reveals link between micro-channel drainage density, surface roughness and surface reflectance. Earth Surf. Process. Landf. 40, 1279-1290.

Scambos, T., Hulbe, C., Fahnestock, M., 2003. Climate-induced ice shelf disintegration in the Antarctic Peninsula, in: Domack, E., Leventer, A., Burnett, A., Bindshadler, R., Convey, P., Kirby, M. (Eds.), Antarctic Peninsula Climate Variability: Historical and Paleoenvironmental Perspectives. Amer Geophysical Union, Washington, pp. 79-92.

Scambos, T.A., Hulbe, C., Fahnestock, M., Bohlander, J., 2000. The link between climate warming and break-up of ice shelves in the Antarctic Peninsula. J. Glaciol. 46, 516-530.

Selmes, N., Murray, T., James, T.D., 2011. Fast draining lakes on the Greenland ice sheet. Geophys. Res. Lett. 38, L15501.

Smith, L.C., Chu, V.W., Yang, K., Gleason, C.J., Pitcher, L.H., Rennermalm, A.K., Legleiter, C.J., Behar, A.E., Overstreet, B.T., Moustafa, S.E., Tedesco, M., Forster, R.R., LeWinter, A.L., Finnegan, D.C., Sheng, Y., Balog, J., 2015. Efficient meltwater drainage through supraglacial streams and rivers on the southwest Greenland ice sheet. Proc. Natl. Acad. Sci. 112, 1001-1006.

Smith, L.C., Yang, K., Pitcher, L.H., Overstreet, B.T., Chu, V.W., Rennermalm, Å.K., Ryan, J., Cooper, M.G., Gleason, C.J., Tedesco, M., Jeyaratnam, J., As, D.v., Broeke, M.R.v.d., Berg, W.J.v.d., Noël, B., Langen, P.L., Cullather, R.I., Willis, M.J., Hubbard, A., Box, J.E., Jenner, B.A., Behar, A.E., 2017. Direct measurements of meltwater runoff on the Greenland ice sheet surface. Proc. Natl. Acad. Sci. 114, E10622-E10631.

Stenborg, T., 1968. Glacier Drainage Connected with Ice Structures. Geografiska Annaler. Series A, Physical Geography 50, 25-53.

Tedesco, M., Willis, I.C., Hoffman, M.J., Banwell, A.F., Alexander, P., Arnold, N.S., 2013. Ice dynamic response to two modes of surface lake drainage on the Greenland ice sheet. Environ. Res. Lett. 8, 034007.

Thomsen, H.H., Thorning, L., Olesen, O.B., 1989. Appplied glacier research for planning hydro-electric power, Ilulissat/Jakobshavn, West Greenland. Ann. Glaciol. 13.

Wright, P.J., Harper, J.T., Humphrey, N.F., Meierbachtol, T.W., 2016. Measured basal water pressure variability of the western Greenland Ice Sheet: Implications for hydraulic potential. J. Geophys. Res. Earth Surf. 121, 1134-1147.

Wyatt, F.R., Sharp, M.J., 2015. Linking surface hydrology to flow regimes and patterns of velocity variability on Devon Ice Cap, Nunavut. J. Glaciol. 61, 387.

Yang, K., Karlstrom, L., Smith, L.C., Li, M., 2017. Automated high resolution satellite image registration using supraglacial rivers on the Greenland Ice Sheet. IEEE J. Sel. Topics Appl. Earth Observ. Remote Sens. 10, 845-856.

Yang, K., Li, M., Liu, Y., Cheng, L., Huang, Q., Chen, Y., 2015a. River detection in remotely sensed imagery using Gabor filtering and path opening. Remote Sens. 7, 8779-8802.

Yang, K., Smith, L.C., 2013. Supraglacial streams on the Greenland ice sheet delineated from combined spectral-shape information in high-resolution satellite imagery. IEEE Geosci. Remote Sens. Lett. 10, 801-805.

Yang, K., Smith, L.C., 2016a. Internally drained catchments dominate supraglacial hydrology of the southwest Greenland Ice Sheet. J. Geophys. Res. Earth Surf. 121, 1891–1910.

Yang, K., Smith, L.C., 2016b. Internally drained catchments dominate supraglacial hydrology of the southwest Greenland Ice Sheet. J. Geophys. Res. Earth Surf. 121, 1891–1910.

Yang, K., Smith, L.C., Chu, V.W., Gleason, C.J., Li, M., 2015b. A caution on the use of surface digital elevation models to simulate supraglacial hydrology of the Greenland Ice Sheet. IEEE J. Sel. Topics Appl. Earth Observ. Remote Sens. 8, 5212-5224.

Yang, K., Smith, L.C., Chu, V.W., Pitcher, L.H., Gleason, C.J., Rennermalm, A.K., Li, M., 2016. Fluvial morphometry of supraglacial river networks on the southwest Greenland Ice Sheet. GISci. Remote Sens. 53, 459-482.

Yang, K., Smith, L.C., Karlstrom, L., Cooper, M.G., Tedesco, M., As, D.v., Cheng, X., Chen, Z., Li, M., 2018. Supraglacial meltwater routing through internally drained catchments on the Greenland Ice Sheet surface. Cryosph. Discuss.

Zwally, H.J., Abdalati, W., Herring, T., Larson, K., Saba, J., Steffen, K., 2002. Surface melt-induced acceleration of Greenland ice-sheet flow. Science 297, 218-222.

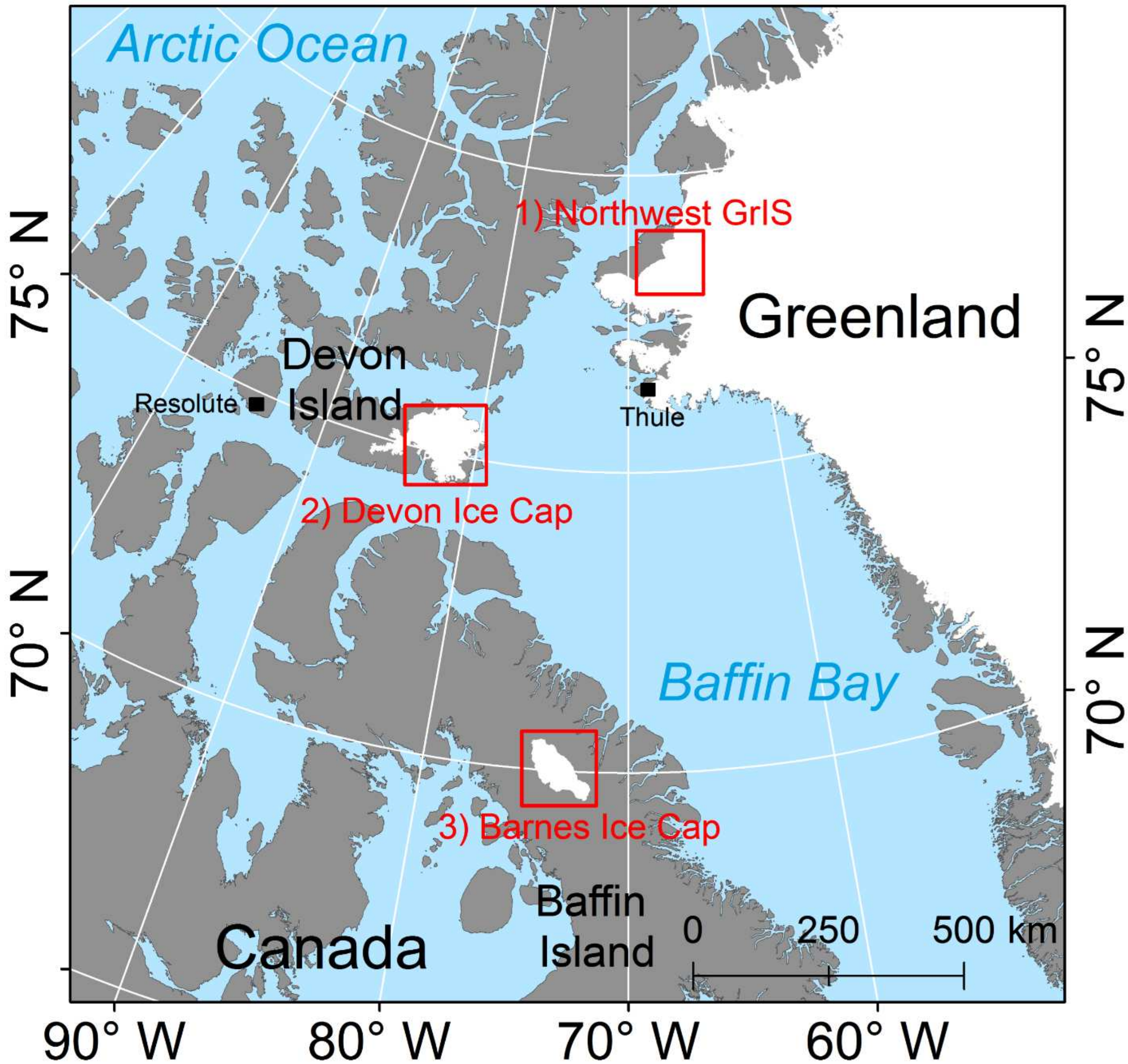

Figure 1. Locations of the three study areas: 1) northwest Greenland Ice Sheet (GrIS), 2) Devon Ice Cap (DIC), and 3) Baffin Ice Cap (BIC).

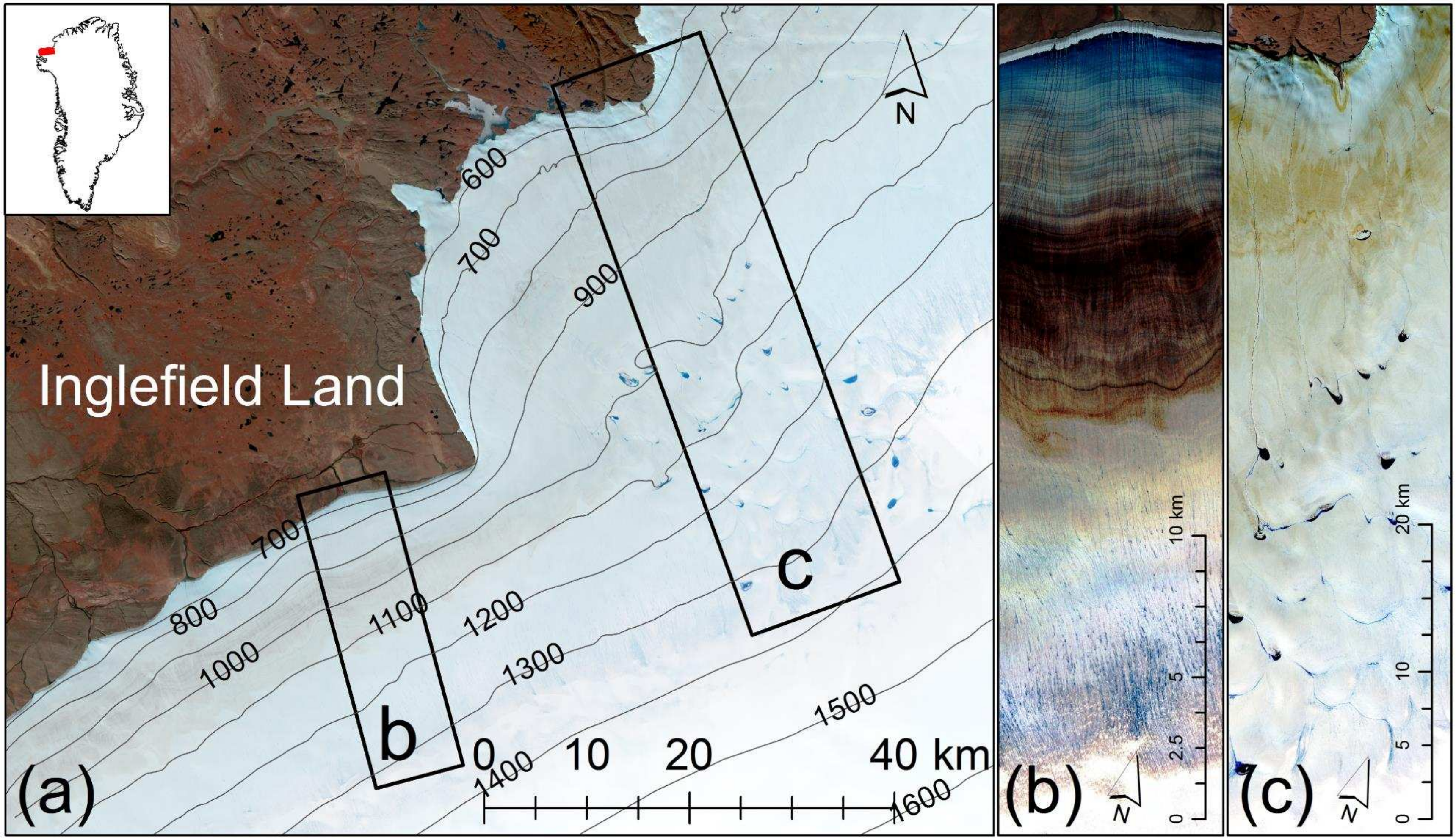

Figure 2. (a) Landsat-8 image (acquired on 30 July 2016, RGB: bands 5 (NIR), 4 (Red), 3 (Green)) of the northwest GrIS. Sentinel-2 images (acquired on 23 July 2016, RGB: bands 8 (NIR), 4 (Red), 3 (Green)) of two typical sites are shown in (b) and (c), indicating continuous supraglacial rivers directly drain meltwater off the ice margin and into proglacial rivers.

623 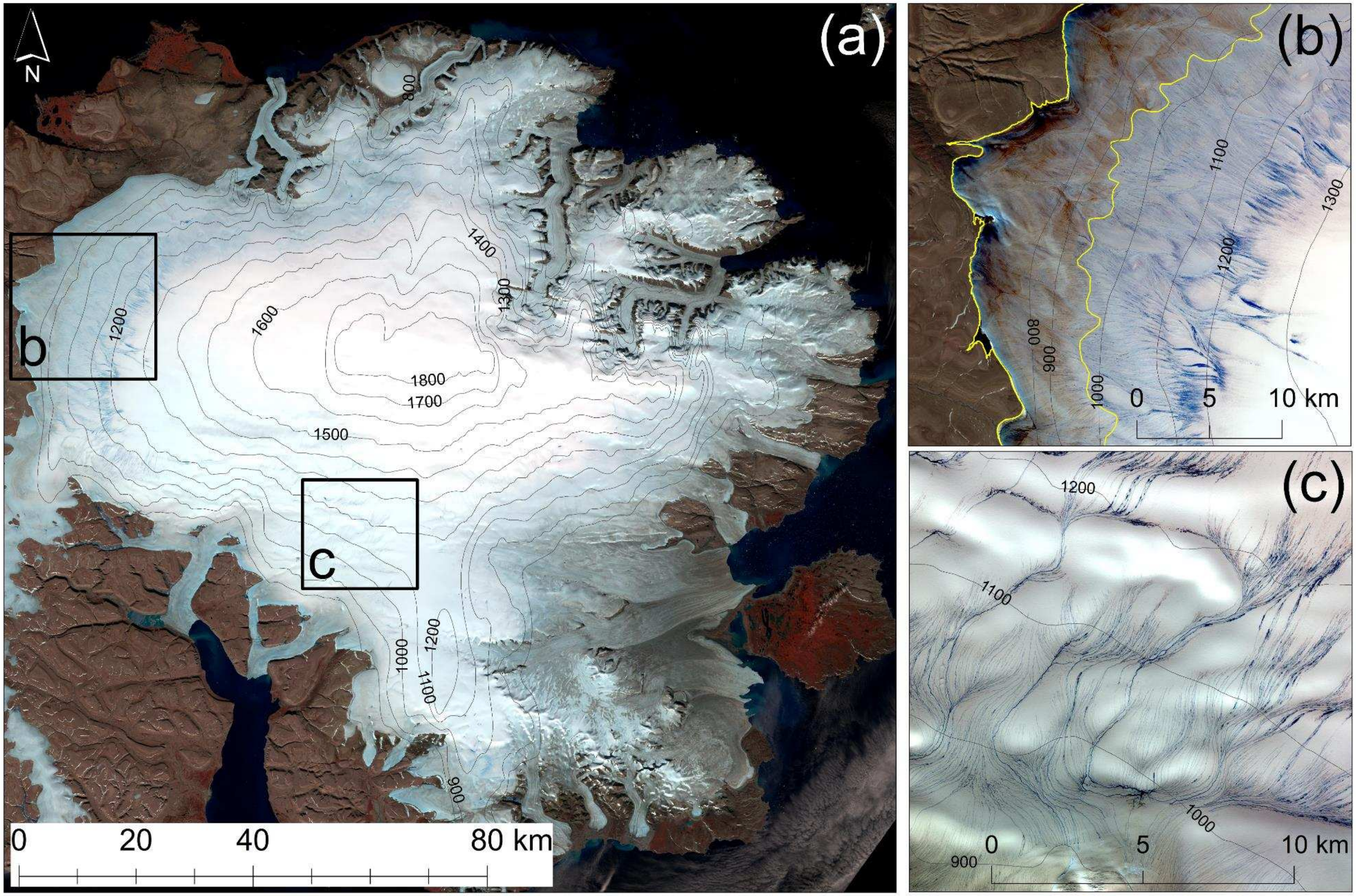
(a)
N
800
1400
1300
1600
1200
b
1800
1700
1500
c
1000
1200
1100
900
0
20
40
80 km
(b)
1100
1300
1200
800
900
1000
0
5
10 km
(c)
1200
1100
1000
0
5
10 km
900

Figure 3. (a) Landsat-8 image (acquired 28 July 2016, RGB: bands 5 (NIR), 4 (Red), 3 (Green)) of the Devon Ice Cap (DIC). Our chosen sites to study ice cap hydrology are (b) western and (c) southern sections of the DIC, shown in two Sentinel-2 images (also acquired 28 July 2016, RGB: bands 8 (NIR), 4 (Red), 3 (Green)). The dark dust zone is enclosed by the yellow line.

628

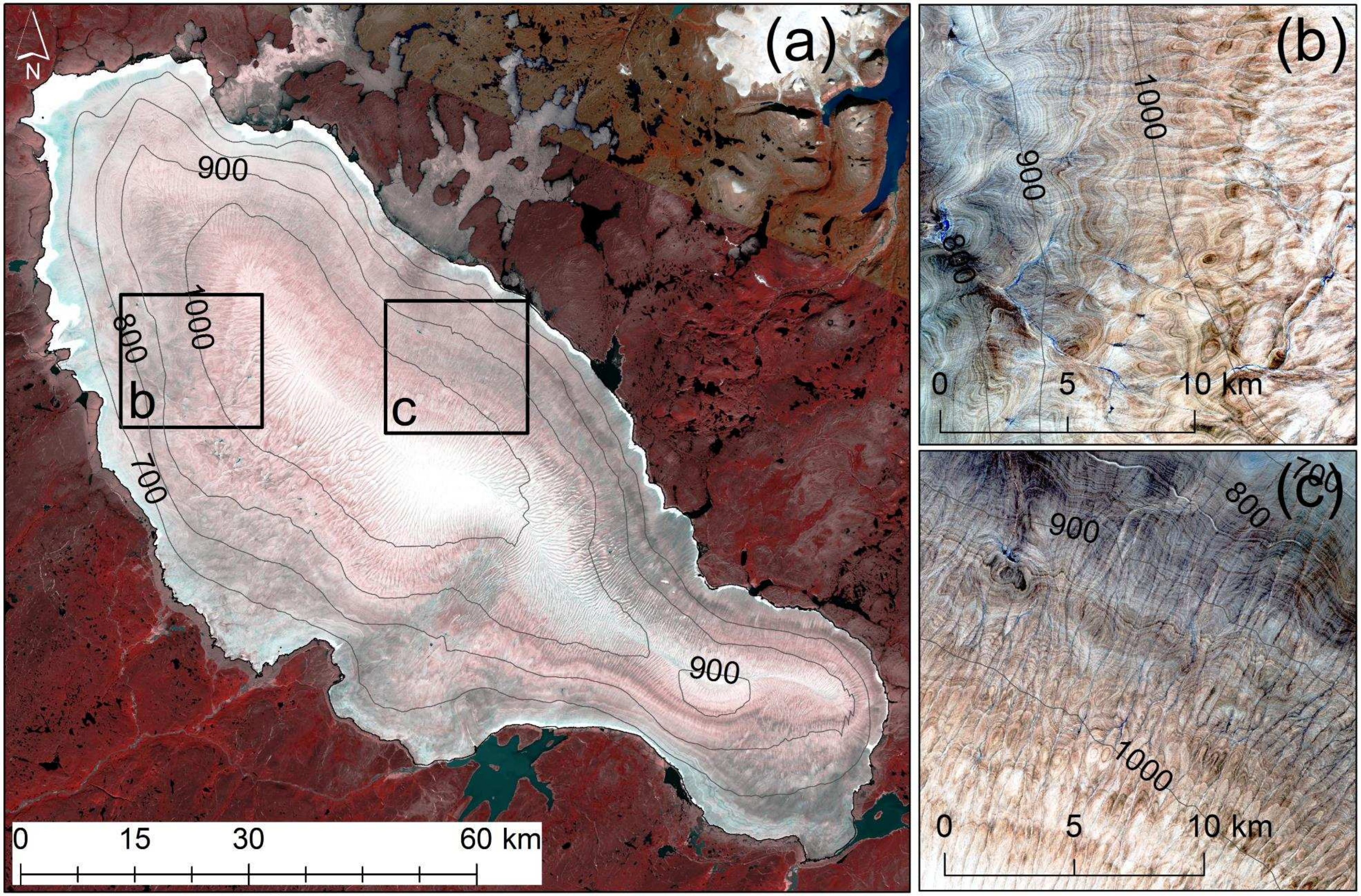

(a)
N
900
1000
800
b
c
700
900
0
15
30
60 km
(b)
1000
900
800
0
5
10 km
(c)
700
800
900
1000
0
5
10 km

Figure 4. (a) Landsat-8 image (acquired on 9 August 2016, RGB: bands 5 (NIR), 4 (Red), 3 (Green)) of the Barnes Ice Cap (BIC). Our chosen sites to study ice cap hydrology are (b) western and (c) eastern sections of the BIC, shown in two Sentinel-2 images (acquired on 20 August 2016, RGB: bands 8 (NIR), 4 (Red), 3 (Green)).

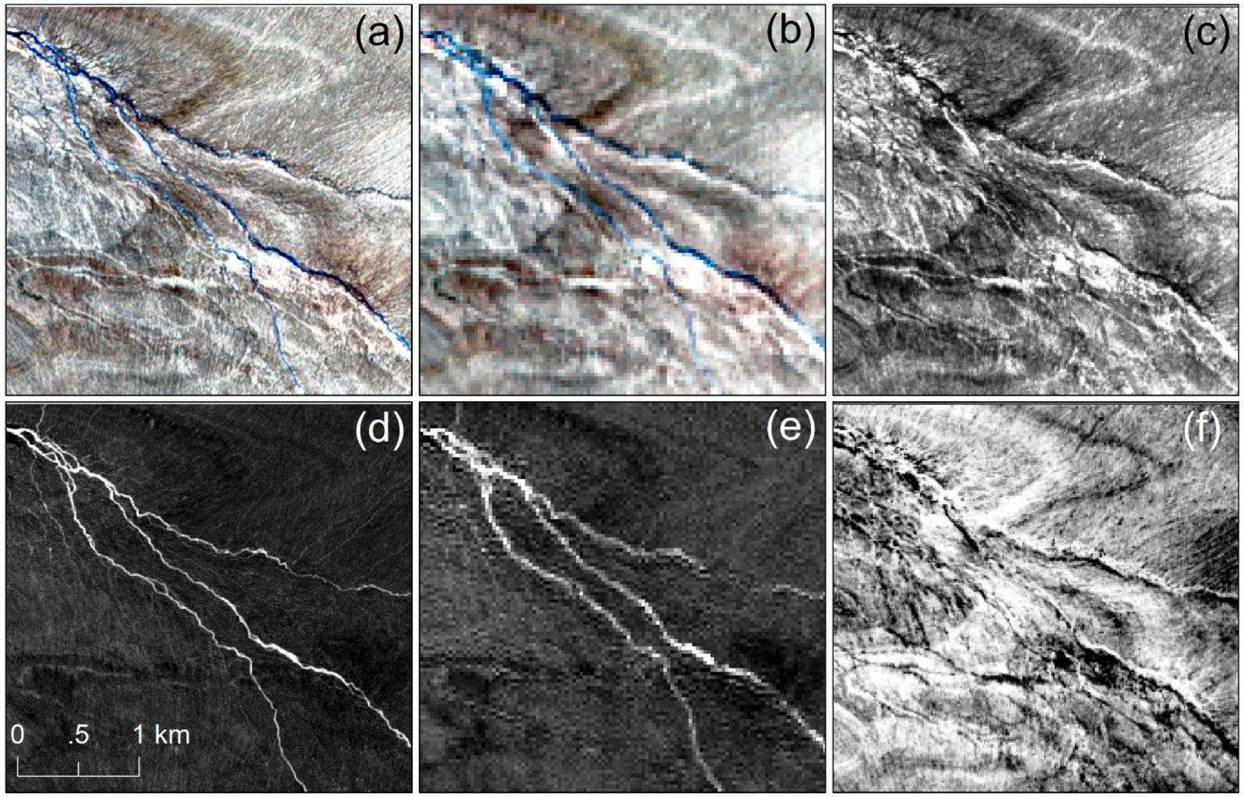

Figure 5. Comparison of supraglacial rivers as detected in (a) 10 m multispectral Sentinel-2 MSI image (acquired on 25 July 2016, RGB: bands 8 (NIR), 4 (Red), 3 (Green)), (b) 30 m multispectral and (c) 15 m panchromatic Landsat-8 OLI imagery (acquired on 26 July 2016). Panels (d) and (e) show the corresponding normalized difference water index (NDWI) images derived from (a) and (b). Panel (f) shows the inverse gray image for the panchromatic image in which meltwater is represented as white color.

638

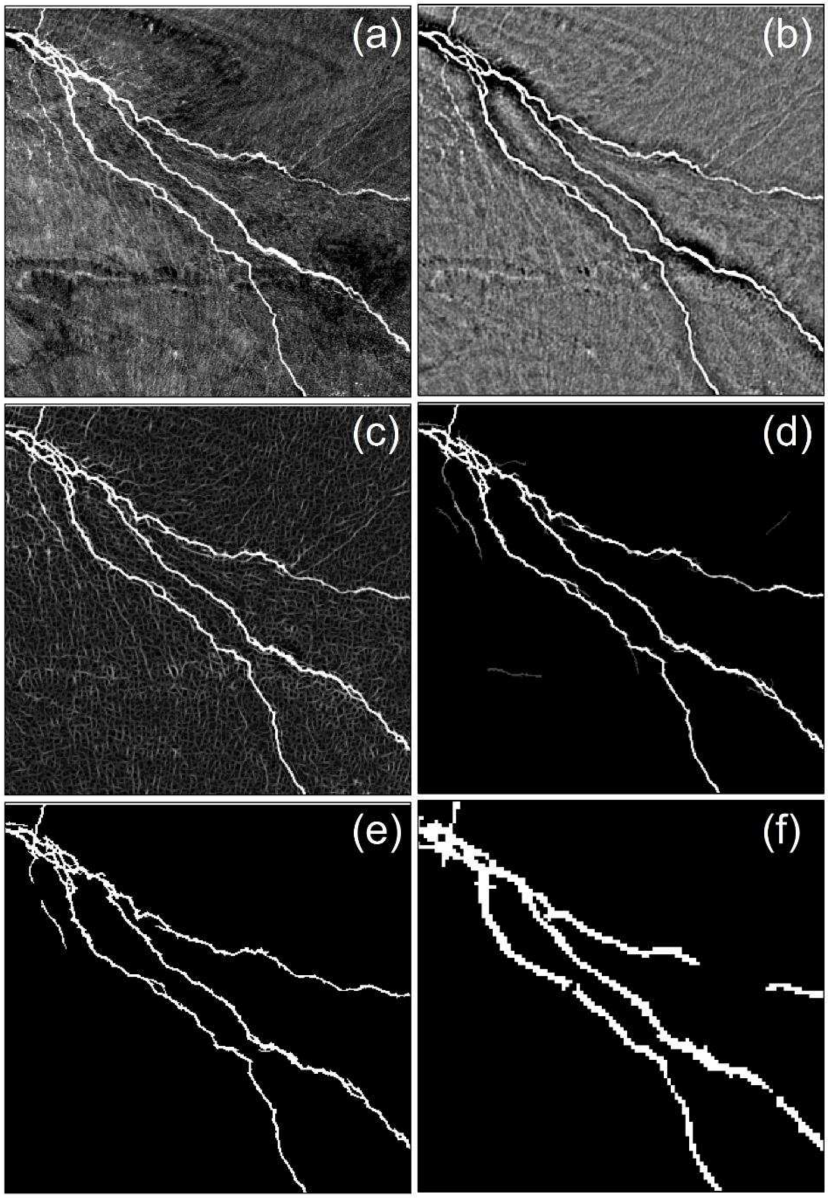

Figure 6. Workflow for delineating a supraglacial river network from 10 m multispectral Sentinel-2 MSI imagery, following the method of Yang et al. (2017): (a) input NDWI image; (b) NDWI image after band-pass DFT filtering; (c) Gabor filtering of (b); (d) enhancement of (c) using a path opening algorithm; (e) final supraglacial river detection results. For comparison, panel (f) shows detection using a contemporary 30 m multispectral Landsat-8 OLI image.

643

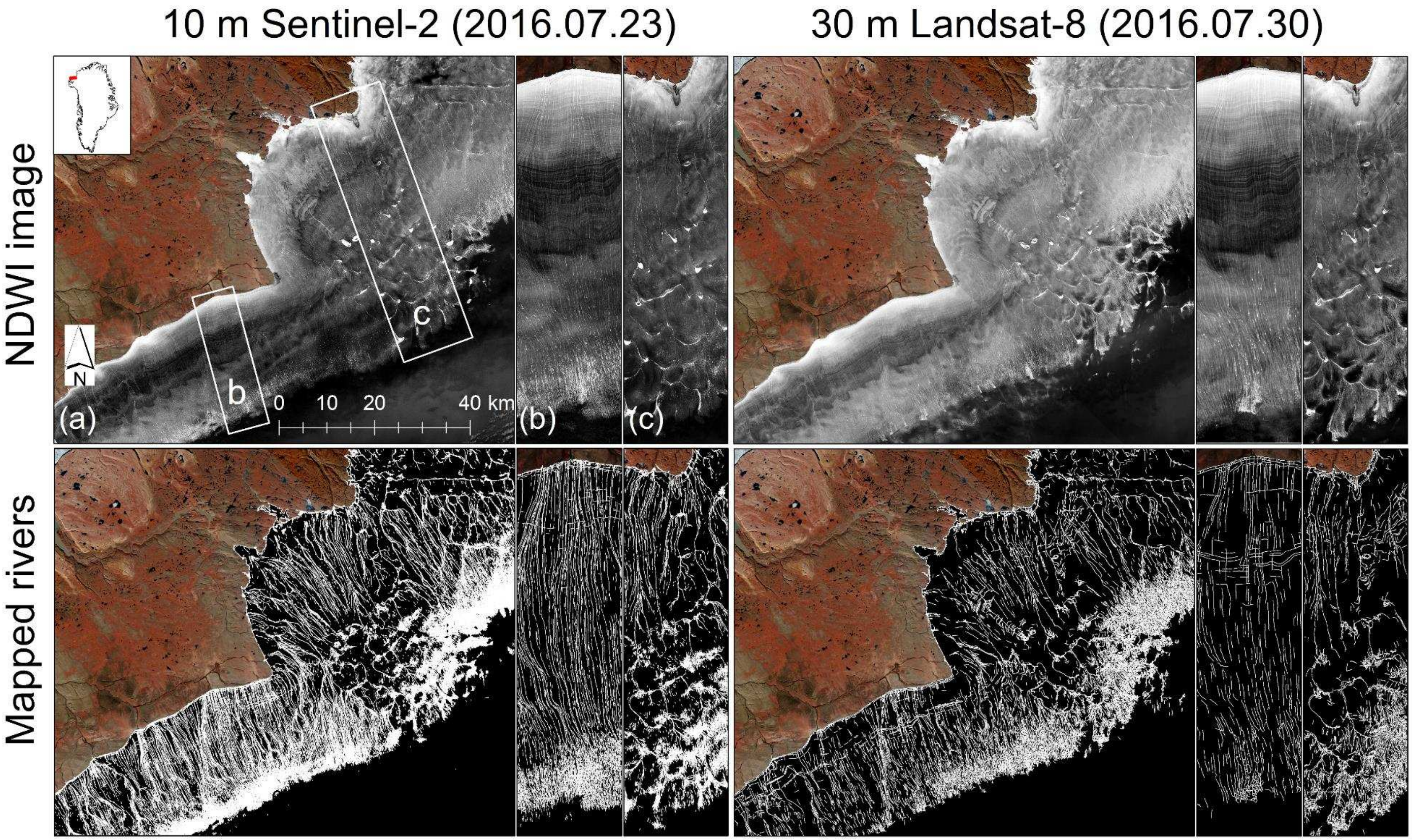

644 **Figure 7**. Supraglacial river networks on the northwest Greenland Ice Sheet near Inglefield Land mapped from two 10 m Sentinel-2 images

645 (acquired on 23 July 2016) and two 30 m Landsat-8 satellite images (acquired on 30 July 2016). Insets reveal (b) long, subparallel supraglacial

rivers flowing ~30 km over the ice to the proglacial zone; and (c) supraglacial rivers interconnecting and draining supraglacial lakes to the proglacial zone.

648

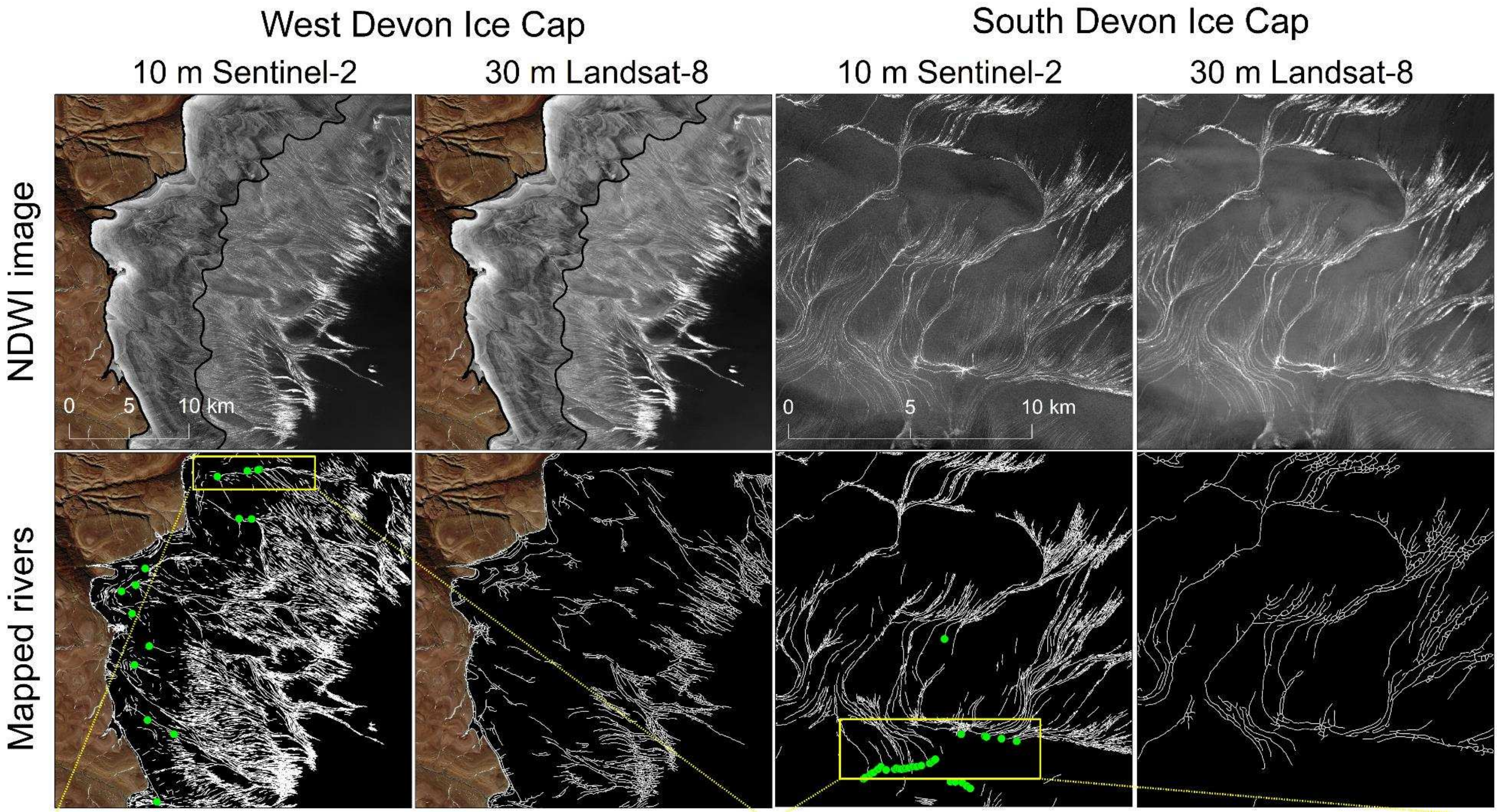
West Devon Ice Cap
South Devon Ice Cap
10 m Sentinel-2
30 m Landsat-8
10 m Sentinel-2
30 m Landsat-8
NDWI image
Mapped rivers
0
5
10 km
0
5
10 km

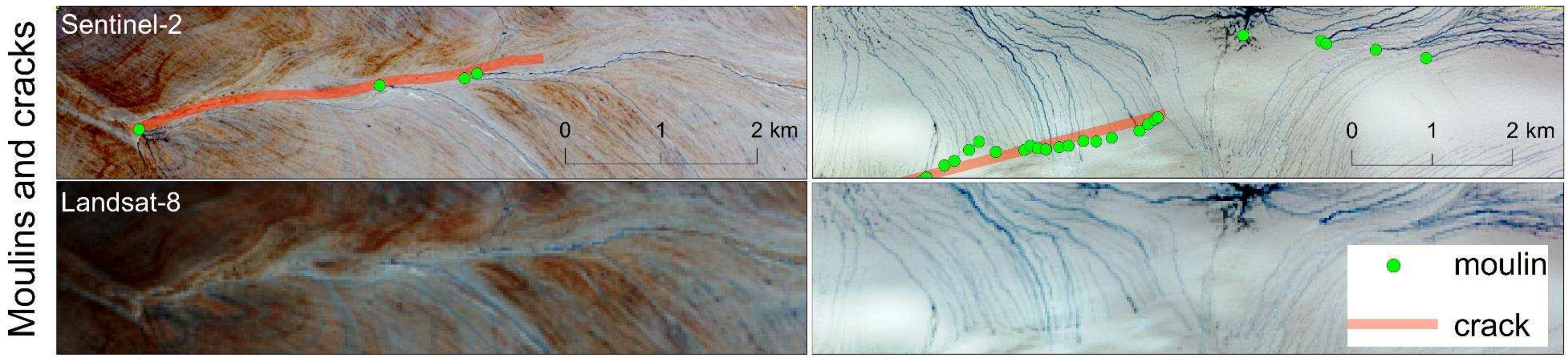

Figure 8. Supraglacial river networks on the western (Figure 2b) and the southern (Figure 2c) sections of the Devon Ice Cap (DIC) mapped from concurrent 10 m Sentinel-2 and 30 m Landsat-8 satellite images (captured on 28 July 2016). Moulins (abrupt terminations of supraglacial river networks) can be reliably identified from the Sentinel-2 images. On the western section of the DIC, straight supraglacial rivers flow continuously toward the ice margin, become more sinuous at low elevations, and are captured by 16 moulins; on the southern section of the DIC, supraglacial rivers are very sinuous and often turn at right angles, indicating strong controls of surface topography. A ~3 km long west-east orientated linear crevasse abruptly terminate supraglacial rivers and form 18 moulins in this small area.

656

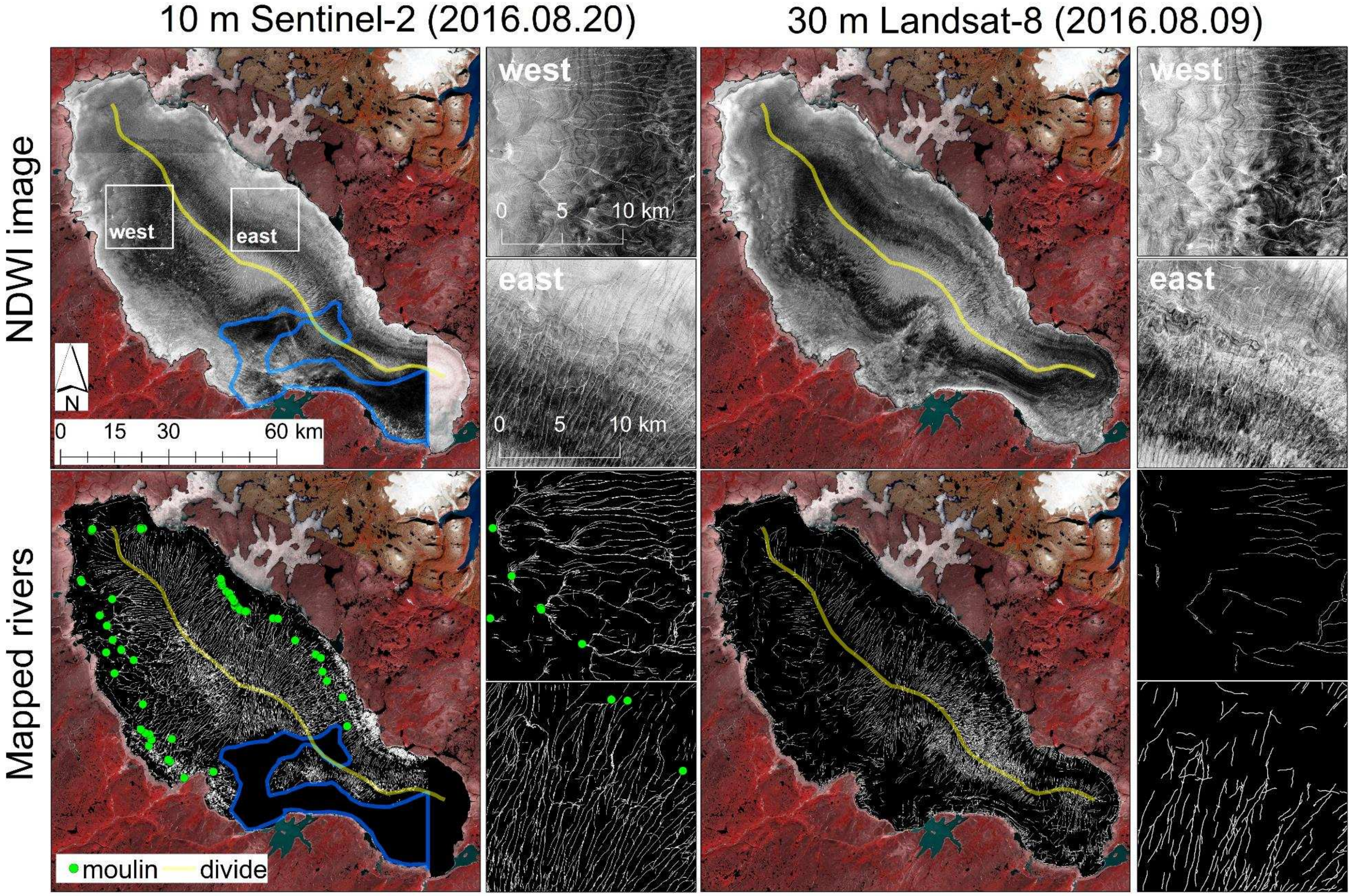

10 m Sentinel-2 (2016.08.20)
30 m Landsat-8 (2016.08.09)
NDWI image
Mapped rivers
west
east
0 5 10 km
0 15 30 60 km
N
moulin
divide

Figure 9. Supraglacial river networks on the Barnes Ice Cap (BIC) mapped from two 10 m Sentinel-2 (captured on 20 August 2016) images and one 30 m Landsat-8 image (captured on 9 August 2016). Two study sites are selected from the western and the eastern sections of the BIC and their corresponding river mapping results are showed in detail. Supraglacial rivers are relatively straight and subparallel on the eastern side, while they are more dendritic on the western side. The yellow line encloses the ice divide and the blue line encloses the area covered by clouds.

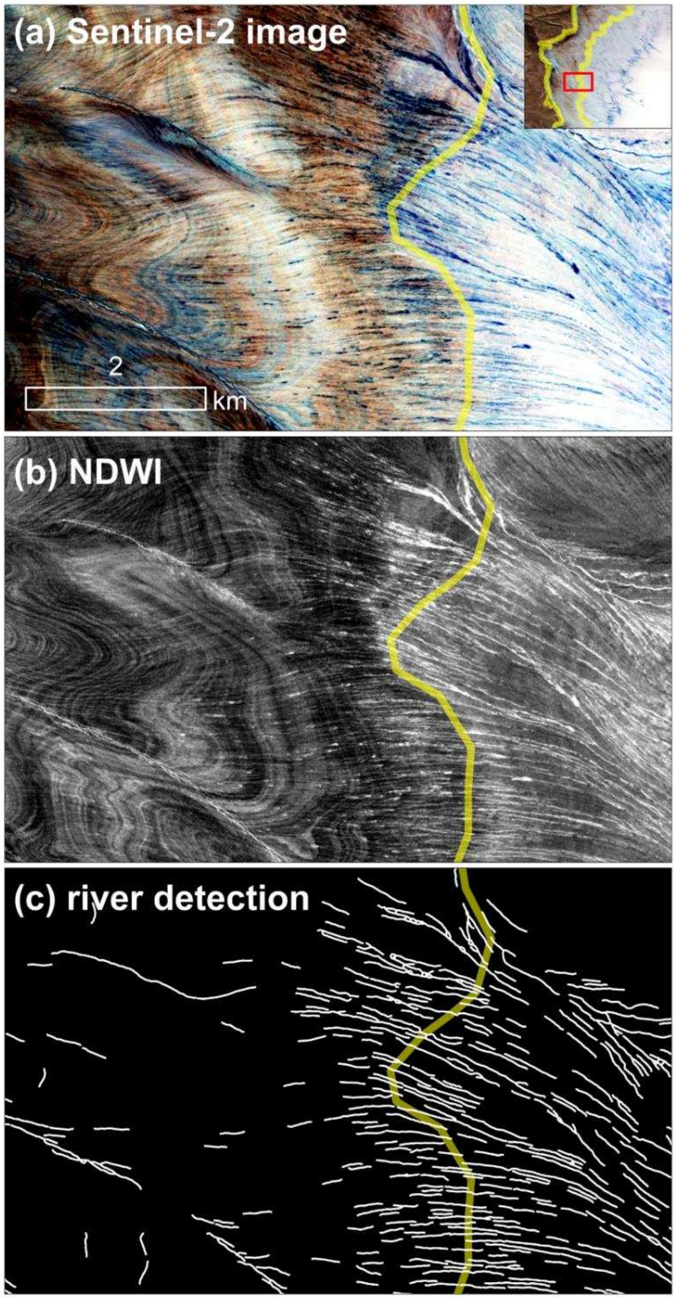

Figure 10. A close-up view of the western section of the Devon Ice Cap (Figure 3b) using (a) Sentinel-2 imagery, (b) derived NDWI image, and (c) meltwater channel detection results, showing “vanishing” of numerous supraglacial rivers after flowing into the dark dust zone. The dark dust zone is enclosed by the yellow line and the inset red outline shows the study area location in the western section of the Devon Ice Cap.

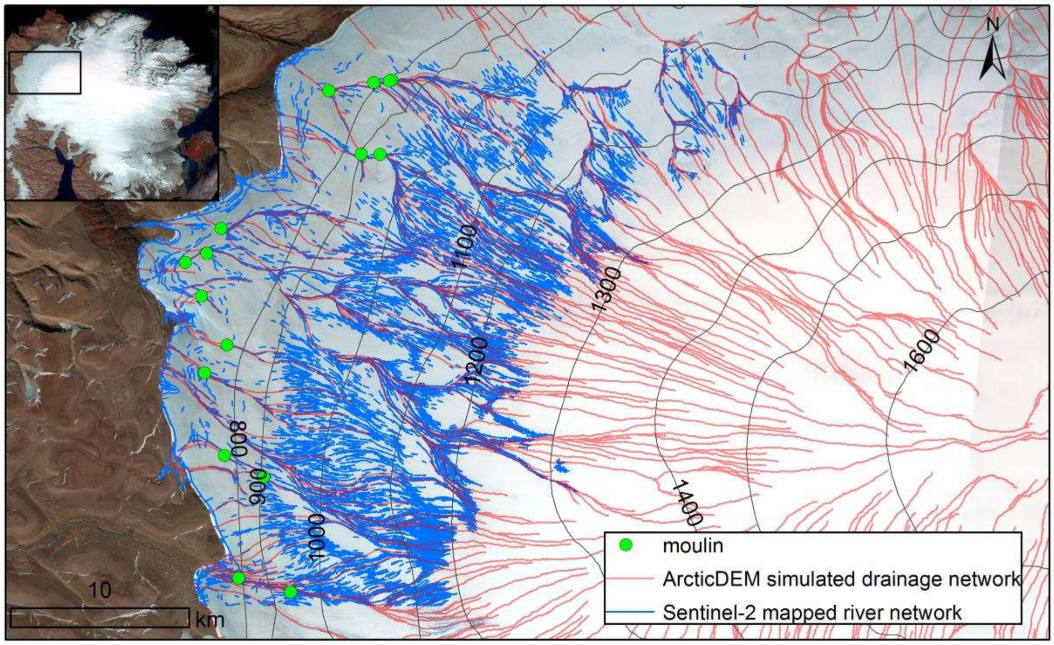

Figure 11. Comparison of ArcticDEM simulated drainage network with Sentinel-2 mapped supraglacial river network for western section of Devon Ice Cap. ArcticDEM simulated drainage networks are more continuous than Sentinel-2 river networks but cannot actual distribution of supraglacial river networks (overestimating high-elevation rivers, underestimating low-elevation rivers, and failing to identify moulins).

Table 1. Sentinel-2 (S2A) and Landsat-8 (LC8) satellite images used in this study.

Study area	Image ID	Acquisition Date
Northwest Greenland Ice Sheet	S2A_OPER_MSI_L1C_TL_SGS__20160723T212906_A005672_T19XEH	2016.07.30
	S2A_OPER_MSI_L1C_TL_SGS__20160723T212906_A005672_T19XDG	2016.07.30
	LC80350032016212LGN00	2016.07.23
	LC80350042016212LGN00	2016.07.23
Devon Ice Cap	S2A_OPER_MSI_L1C_TL_SGS__20160728T220647_A005744_T16XEJ	2016.07.28
	S2A_20160728T220647_A005744_T17XMD	2016.07.28
	LC80370072016210LGN00	2016.07.28
Barnes Ice Cap	S2A_OPER_MSI_L1C_TL_MTI__20160820T221251_A006072_T18WWC	2016.08.20
	S2A_OPER_MSI_L1C_TL_MTI__20160820T221251_A006072_T18WWD	2016.08.20
	LC80250112015222LGN00	2016.08.09

Table 2. Statistics of supraglacial rivers mapped from Sentinel-2 and Landsat-8 images for the northwest Greenland Ice Sheet (GrIS), the Devon Ice Cap, and the Barnes Ice Cap.

Study area		**Area (km^2)**	**Total river length (km)**		**Drainage density (km^{-1})**	
			Sentinel-2	**Landsat-8**	**Sentinel-2**	**Landsat-8**
Northwest GrIS		4281.4	24010.0	11440.2	5.6	2.7
Devon Ice Cap	**West**	561.7	2866.5	951.2	5.1	1.7
	South	200.1	661.5	292.6	3.3	1.5
Barnes Ice Cap		4660.3*	11653	7282.8	2.5	1.3

*The total area of the Barnes Ice Cap is 5736.2 km^2. The Sentinel-2 images miss a small east portion (280.8 km^2) and clouds cover an area of 795.2 km^2 (see blue line in Figure 9), both of which are excluded from the actual mapped area.